https://doi.org/10.31891/2307-5732-2026-361-44
УДК 621.314

DENYS KHOMIUK
Lviv Polytechnic National University
https://orcid.org/0009-0001-5599-5426
e-mail: denys.s.khomiuk@lpnu.ua
SAMOTYY VOLODYMYR
Lviv Polytechnic National University
https://orcid.org/0000-0003-2344-2576
e-mail: volodymyr.v.samotyy@lpnu.ua

MATHEMATICAL MODELING AND A TECHNIQUE FOR GENERATING A SPECIFIED OUTPUT VOLTAGE WAVEFORM IN A SINGLE-PHASE THYRISTOR FREQUENCY CONVERTER

This paper presents a comprehensive study focused on the development of a mathematical model and a high-performance hysteresis-based control technique for a single-phase thyristor frequency converter. The primary objective of the research is to enable the synthesis of an arbitrary output voltage waveform, thereby enhancing the functional capabilities of thyristor-based topologies which are traditionally limited by their latching characteristics. The investigated converter architecture is a two-stage AC-DC-AC system comprising three critical functional blocks: a full-wave controlled rectifier utilizing a center-tapped transformer, an intermediate DC link implemented as an LC filter with a smoothing choke, and a parallel bridge inverter equipped with a specific commutating capacitor. This commutating capacitor is essential for the forced commutation required to implement flexible control strategies on thyristor switches.

To accurately analyze the complex electromagnetic processes within this system, the authors derive a rigorous mathematical model based on a state-space representation. The model utilizes a system of nonlinear differential equations that incorporate logical variables to dynamically represent the variable topology of the circuit induced by the switching states of the thyristors. These logical variables act as multipliers for system coefficients, allowing the model to seamlessly transition between different structural configurations, such as the conduction states of the rectifier valves and the inverter bridge pairs within a single set of equations. The state vector comprehensively includes magnetic flux linkages of the transformers, winding currents, and voltages across the filter and commutating capacitors.

The proposed control strategy is a hybrid approach that concurrently governs both power stages. The rectifier is regulated via phase-angle control, where the firing angle is adjusted to modulate the DC link voltage. Conversely, the inverter stage employs a non-linear hysteresis control law. This technique continuously compares the instantaneous output voltage across the commutating capacitor with a predefined arbitrary reference signal. By maintaining the error within a specific tolerance band, the controller generates switching commands that force the output voltage to track the reference waveform with high fidelity.

To validate the theoretical model and control algorithm, numerical simulations were conducted using the adaptive-step Runge-Kutta-Fehlberg (RKF45) method. The performance was evaluated across a spectrum of operating frequencies, including 50 Hz, 150 Hz, and 500 Hz. The results demonstrate that the system achieves smooth transients and precise sinusoidal waveform generation at low frequencies. Furthermore, at higher frequencies (500 Hz), the converter exhibits exceptional robustness and fast dynamic response, with the hysteresis controller effectively constraining the voltage within the tolerance band despite the increased load dynamics. This research bridges a significant gap in the application of non-linear control to thyristor-based converters, offering a viable solution for improving power quality in grid-connected renewable energy systems and advanced industrial applications requiring precise waveform synthesis.

Keywords: *thyristor frequency converter, mathematical modeling, hysteresis-based control, phase-angle control.*

ХОМЮК ДЕНИС, САМОТИЙ ВОЛОДИМИР
Національний університет «Львівська Політехніка»

МАТЕМАТИЧНА МОДЕЛЬ ТА МЕТОДИКА ФОРМУВАННЯ ВИХІДНОЇ НАПРУГИ ЗАДАНОЇ ФОРМИ В ОДНОФАЗНОМУ ТИРИСТОРНОМУ ПЕРЕТВОРЮВАЧІ ЧАСТОТИ

У цій статті представлено математичну модель та техніку гістерезисного керування для однофазного тиристорного перетворювача частоти, призначеного для синтезу напруги заданої форми. Перетворювач складається з керованого двопівперіодного випрямляча з трансформатором із середньою точкою, фільтра ланцюга постійного струму типу LC та паралельного інвертора з комутуючим конденсатором. Модель базується на представленні в просторі станів із нелінійними диференціальними рівняннями, які включають логічні змінні для відображення змінної топології, зумовленої станами комутації тиристорів, зокрема магнітними потокозчепленнями, струмами обмоток і напругами на конденсаторах.

Фазове керування регулює вихідну напругу випрямляча, тоді як гістерезисне керування інвертора забезпечує перемикання пар тиристорів для утримання вихідної напруги в межах заданого діапазону навколо візрцевого сигналу. Чисельна симуляція оцінює продуктивність при різних робочих частотах, демонструючи плавні перехідні процеси та високу точність синусоїдальної форми напруги на низьких частотах із швидким затуханням коливань; на вищих частотах система продовжує демонструвати надійну продуктивність та високоточне відстеження, демонструючи широку робочу смугу пропускання та швидку динамічну реакцію методу керування.

Ця робота заповнює прогалину в застосуванні нелінійного керування до схем із тиристорними топологіями для точного модулювання форми напруги вихідного сигналу, сприяючи підвищенню якості електроенергії в системах з'єднання з мережею відновлюваних джерел та інших застосуваннях.

Ключові слова: *тиристорний перетворювач частоти, математичне моделювання, гістерезисне керування, фазове керування.*

Стаття надійшла до редакції / Received 13.12.2025
Прийнята до друку / Accepted 11.01.2026
Опубліковано / Published 29.01.2026

Problem statement and analysis of research and publications

Single-phase AC-AC power converters are fundamental components in modern electrical systems, serving as the critical interface for grid-connected renewable energy sources, uninterruptible power supplies (UPS), and advanced industrial processes [1, 2]. The increasing prevalence of sensitive electronic loads and stringent grid interconnection standards has intensified the demand for converters that not only ensure efficient power transfer but also actively enhance power quality by synthesizing a high-fidelity sinusoidal output voltage [3, 4]. The primary challenge lies in achieving this with exceptional dynamic performance, ensuring rapid and stable response to abrupt changes in load or reference commands. This requirement has driven extensive research into advanced control strategies for the voltage source inverter (VSI), which constitutes the core of most AC-AC conversion systems.

The dominant industrial approach for VSI control is based on linear control theory coupled with high-frequency Pulse-Width Modulation (PWM) [5, 6]. In this paradigm, controllers such as the Proportional-Resonant (P-Res) type are employed to track a sinusoidal reference with zero steady-state error, generating a control signal that modulates a fixed-frequency carrier wave to produce the inverter switching commands [4, 7]. This method's primary advantage is its well-defined harmonic spectrum, with distortion concentrated at multiples of the switching frequency, which simplifies the design of output filters [6]. However, the dynamic response of linear PWM systems is fundamentally constrained by the controller bandwidth and sampling period, limiting their performance in applications requiring instantaneous corrective action [8]. An alternative lies in non-linear control techniques, most notably hysteresis (or bang-bang) control. This strategy offers an unparalleled dynamic response, inherent robustness, and implementation simplicity by directly switching the inverter states to maintain the output voltage error within a predefined hysteresis band [9, 10]. This instantaneous, event-driven action circumvents the bandwidth limitations of linear controllers, but at the cost of a variable switching frequency, which produces a wideband harmonic spectrum that complicates filter design and electromagnetic interference (EMI) mitigation [9, 11].

The practical implementation of such high-frequency, forced-commutation control strategies is intrinsically linked to the evolution of power semiconductor technology. Conventional thyristors, or Silicon-Controlled Rectifiers (SCRs), are latching devices that can only be turned off when their current naturally commutates to zero. This characteristic makes them unsuitable for algorithms that demand turn-off at arbitrary instants. The development of fully controllable switches was therefore a critical enabler. The Gate Turn-Off Thyristor (GTO) was an early breakthrough, but it suffered from slow switching speeds, high losses, and the need for complex, high-power gate drive circuits to supply a large negative current pulse for turn-off [12, 13]. The modern Insulated-Gate Bipolar Transistor (IGBT) has largely superseded the GTO in new designs, offering a superior combination of high-power handling, fast switching speeds, and a simple, low-power, voltage-controlled gate, making it the de facto standard for high-performance inverters [14, 15]. The Integrated Gate-Commutated Thyristor (IGCT), an advanced GTO derivative, also offers improved performance for very high-power applications [16].

This analysis reveals a distinct research gap. While hysteresis control is a well-established technique for standard IGBT-based VSIs, its application to converter topologies that utilize thyristor-based power stages for the specific purpose of high-fidelity arbitrary waveform generation remains largely unexplored. Existing mathematical models for thyristor converters typically focus on line-commutated operation for rectification and do not address the dynamics of high-frequency, forced-commutation control for precise voltage synthesis. Therefore, the primary contribution of this work is the development, mathematical modeling, and performance analysis of a single-phase frequency converter that uniquely integrates a thyristor-based power stage with a high-performance, non-linear hysteresis voltage control technique. The objectives are to: (1) derive a comprehensive mathematical model of the proposed AC-DC-AC converter suitable for time-domain simulation; (2) formalize and implement the hysteresis-based control law to generate a specified output voltage waveform; and (3) analyze the system's performance, focusing on key metrics such as waveform fidelity, dynamic response, and the resultant switching frequency characteristics.

Formulation of the goals of the article

The purpose of the article is to develop a mathematical model and propose a control technique for a single-phase thyristor frequency converter. The proposed technique enables the synthesis of an output voltage with a predefined, arbitrary waveform by tracking a reference signal, thereby improving the output quality and expanding the functional capabilities of the converter.

Mathematical model of the single-phase thyristor frequency converter

The schematic diagram of the single-phase thyristor frequency converter under consideration is presented in Fig 1. This device is designed to perform a two-stage AC-DC-AC power conversion, transforming a single-phase AC input of a fixed frequency into a single-phase AC output with a controllable, user-defined waveform and frequency.

Structurally, the converter consists of three primary functional blocks connected in series: a controlled rectifier, an intermediate DC link filter, and a bridge parallel inverter. The input stage is a single-phase, full-wave controlled rectifier based on a transformer with a center-tapped secondary, thyristors T_1 and T_2, and a filter capacitor C. This stage converts the input AC voltage U_1 into a controllable DC voltage U_C. This voltage is then smoothed by the DC link, an LC filter composed of the capacitor C and a smoothing choke L_{Ch}. The DC link provides a stable DC power source for the output stage. The final block is a bridge parallel thyristor inverter, which includes a thyristor H-bridge (T_3-T_6), a commutating capacitor C_C, and an output transformer. This stage synthesizes the final AC output voltage U_{Cc} by sequentially switching the thyristors according to a specific control algorithm.

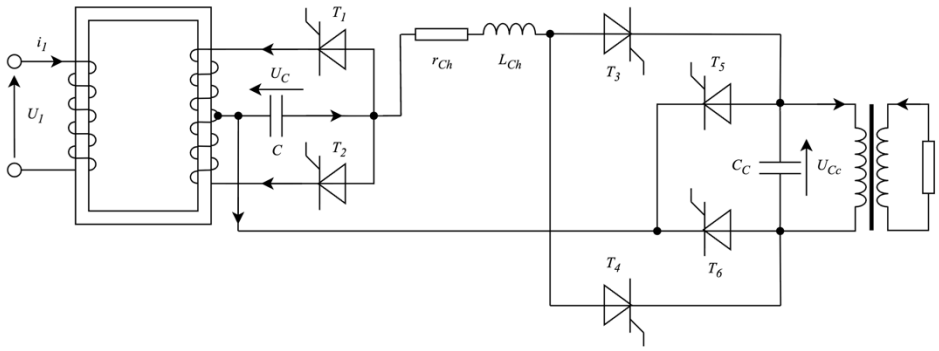

Fig. 1. Schematic diagram of the single-phase thyristor frequency converter

The dynamic behavior of this converter is determined by the complex electromagnetic interactions within and between these stages. To accurately analyze these processes, a mathematical model is derived. The converter is broken down into its functional nodes—the controlled rectifier, the DC link, and the parallel bridge inverter—with the semiconductor valves represented by an ideal switch model.

The input stage is a full-wave rectifier with two controlled valves (T_1, T_2) and a center-tapped transformer. Its model is built upon generalized equations for the three possible combinations of valve states (T_1 open, T_2 open, or both closed). To generalize this behavior, logical variables k_1 and k_2 are introduced, representing the states of thyristors T_1 and T_2, respectively. These variables take a value of 0 for a closed valve and 1 for an open valve.

The equations describing the magnetic state of the rectifier's transformer and the currents in its secondary windings, i_{r21} and i_{r22}, are written in a general form:

$$\frac{d\psi_r}{dt} = g_{r1}\frac{d\Psi_{r1}}{dt} + g_{r21}\frac{d\Psi_{r21}}{dt} + g_{r22}\frac{d\Psi_{r22}}{dt} \quad (1)$$

$$\frac{di_{r21}}{dt} = a_{r21}\frac{d\Psi_{r1}}{dt} + a_{r22}\frac{d\Psi_{r21}}{dt} \quad (2)$$

$$\frac{di_{r22}}{dt} = a_{r31}\frac{d\Psi_{r1}}{dt} + a_{r33}\frac{d\Psi_{r22}}{dt} \quad (3)$$

where ψ_r is the working magnetic flux linkage of the rectifier's transformer, and Ψ_{r1}, Ψ_{r21}, Ψ_{r22} are the total flux linkages of its windings. The g_r and a_r coefficients depend on the instantaneous saturation state of the core and are directly modulated by the logical variables k_1 and k_2. These variables act as multipliers within the expressions for the coefficients, effectively including or excluding terms associated with a particular circuit branch based on whether its corresponding thyristor is conducting. This approach allows a single set of equations to dynamically represent the variable topology of the rectifier as the thyristors switch.

The equation for the voltage U_C across capacitor C accounts for the current it delivers to the choke, i_{Lch}:

$$\frac{dU_C}{dt} = \frac{1}{C}(i_{r21} + i_{r22} - i_{Lch}) \quad (4)$$

The DC link consists of the choke L_{Ch}, and the inverter is composed of a thyristor bridge (T_3-T_6) and a commutating capacitor C_C. The inverter's operation is described by the logical variable ε, which takes values of ± 1 depending on which diagonal pair of thyristors is conducting. A value of $\varepsilon = +1$ signifies that thyristors T_3 and T_6 are conducting, while $\varepsilon = -1$ signifies that thyristors T_4 and T_5 are conducting.

The equation for the choke current i_{Lch}, considering the rectifier's capacitor voltage U_C as the source and the commutating capacitor voltage U_{Cc} as the counter-EMF, is:

$$\frac{di_{Lch}}{dt} = \frac{1}{L_{Ch}}(U_C - \varepsilon U_{Cc} - r_{Ch}i_{Lch}) \quad (5)$$

The voltage U_{Cc} on the commutating capacitor C_C is determined by the choke current (charging) and the primary current of the output transformer (discharging):

$$\frac{dU_{Cc}}{dt} = \frac{1}{C_c}(\varepsilon i_{Lch} - i_{inv1}) \quad (6)$$

The inverter's output transformer is modeled by equations for its working flux linkage ψ_{inv} and primary winding current i_{inv1}. The voltage applied to the primary winding is the voltage across the commutating capacitor, U_{Cc}.

$$\frac{d\psi_{inv}}{dt} = D_{inv}(U_{inv} - R_{inv}I_{inv}) \quad (7)$$

$$\frac{di_{inv1}}{dt} = A_{inv1}(U_{inv} - R_{inv}I_{inv}) \quad (8)$$

where $U_{inv} = (U_{Cc}, 0)^T; I_{inv} = (i_{inv1}, i_{inv2})^T$

By combining the derived differential equations (1-8), a system of state equations is formed for the entire frequency converter. The state vector X is defined comprehensively to include all variables that describe the system's energy storage elements across all possible operating modes:

$$X = [\psi_r, i_{r21}, i_{r22}, U_C, i_{Lch}, \psi_{inv}, i_{inv1}, U_{Cc}]^T$$

It is important to note that while the state vector has a fixed size for modeling purposes, some of its components become inactive depending on the converter's switching state. For instance, the rectifier currents $i_{r21}$and i_{r22} are only dynamic when their corresponding thyristors are conducting. The resulting system of state equations that describes the converter's dynamics is a system of nonlinear differential equations with a variable structure, determined by the combinations of the logical variables k_1, k_2, ε. Further analysis of the converter's transient and steady-state operating modes is performed by numerically integrating this system.

Control technique for the single-phase thyristor frequency convert

The control of the frequency converter is implemented as a set of rules that govern the switching of all thyristors. The strategy is divided into two distinct but concurrent algorithms for the rectifier and inverter stages, which together provide complete governance over the converter. Following the physical structure of the device, the control of the rectifier is described first.

The control of the rectifier thyristors (T_1, T_2) is based on the principle of phase angle control, which allows for the regulation of the average DC voltage supplied to the DC link. This is achieved by intentionally delaying the turn-on signal for each thyristor by a specific firing angle (α) relative to the zero-crossing of the input AC voltage. The firing angle α is the primary control parameter for the rectifier. It can be adjusted (e.g., from 0° to 180°) to modulate the power flow. A smaller firing angle results in a higher average DC voltage, while a larger angle reduces it.

The switching conditions for thyristor T_1 (variable k_1) are therefore defined as follows:

1. Turn-on Condition ($k_1 \to 1$): Thyristor T_1 is switched on only when two conditions are met simultaneously:
   a. The thyristor is forward-biased ($u_{d1} > 0$).
   b. The phase of the input AC voltage has reached the specified firing angle ($\omega t(mod 2\pi) \geq \alpha$). This condition is checked only when the thyristor is in the off state ($k_1 = 0$).
2. Turn-off Condition **($k_1 \to 0$):** Thyristor T_1 is line-commutated, meaning it turns off naturally when its current, i_{r21}, attempts to reverse. This condition, $i_{r21} \leq 0$, is checked only when the thyristor is in the on-state ($k_1 = 1$).

The switching conditions for thyristor T_2 (variable k_2) are analogous for the negative half-cycle of the input voltage. This active control of the rectifier stage is crucial for implementing advanced strategies, such as maintaining a constant DC link voltage under varying load conditions.

The primary objective of the inverter control is to ensure that the output voltage across the commutating capacitor, U_{Cc}, accurately tracks a predefined reference signal, $u_{ref}(t)$. The reference signal is defined as:

$$u_{ref}(t) = U_{m,ref} \cdot f(t)$$

where $U_{m,ref}$ is the target amplitude and $f(t)$ defines the desired waveform. This is achieved using a hysteresis control method. The instantaneous output voltage $U_{Cc}(t)$ is continuously compared to the reference, and a tolerance band, or hysteresis window, is defined around the reference signal as $\left[u_{ref}(t) - \Delta U_{tol}, u_{ref}(t) + \Delta U_{tol}\right]$.

The switching logic for the inverter thyristor pairs, represented by the logical variable ε, is determined by whether the output voltage attempts to exit this band:

1. If $U_{Cc}(t) > u_{\text{ref}}(t) + \Delta U_{tol}$ the voltage has exceeded the upper bound. To decrease the voltage, the opposing thyristor pair is activated by setting $\varepsilon = -1$ (turning on T_4 and T_5).
2. If $U_{Cc}(t) < u_{\text{ref}}(t) + \Delta U_{tol}$ the voltage has fallen below the lower bound. To increase the voltage, the primary thyristor pair is activated by setting $\varepsilon = +1$ (turning on T_3 and T_6).

This high frequency switching forces the output voltage to remain within the tolerance band, thus replicating the reference waveform. Together, the phase-angle control of the rectifier and the hysteresis control of the inverter provide complete governance over the converter's operation.

Numerical simulation results

To validate the developed mathematical model and evaluate the performance of the control algorithm, a numerical simulation of the frequency converter's operation was performed. The simulation was conducted over a single period interval $T = 0.02$s using the following component parameters: input voltage $U_1 = 311sin(2\pi f_{in}t)$ V, $f_{in} = 50$ Hz; rectifier filter capacitor $C = 5$ μF with resistance $r_1 = 16.2$ Ω, $r_{21} = r_{22} = 15.8$ Ω, $\alpha_1 = 5$ H^{-1}, $\alpha_{21} = \alpha_{22} = 10$ H^{-1}; smoothing choke $L_{Ch} = 10$ mH with resistance $r_{Ch} = 500$ Ω; invertor commutating capacitor $C_c = 25$ μF, $r_{inv1} = 3.14$ Ω, $r_{inv2} = 3.62$ Ω, $\alpha_{inv1} = 75$ H^{-1}, $\alpha_{inv2} = 100$ H^{-1} The parameters for both transformers were defined by their winding resistances and magnetization curves, which account for magnetic saturation. The magnetization curve is approximated by an expression with the choice of a computational formula:

$$\varphi(\psi) = \begin{cases} a_1\psi, & |\psi| > \psi_1, \\ S_3(\psi), & \psi_1 \leq |\psi| \leq \psi_2 \\ a_2\psi - a_0, & |\psi| > \psi_2 \end{cases}$$

where $a_1 = 0.25$ H^{-1}; $a_2 = 3.0$ H^{-1}; $a_0 = 1.8$ A; $\psi_1 = 0.2$ Wb; $\psi_2 = 0.9$ Wb; $\varphi(\psi_1) = 0.05$ A; $\varphi(\psi_2) = 0.9$ A; $S_3(\psi)$ is a cubic spline. Note that $\alpha''(\psi_1) = a_1$, $\alpha''(\psi_2) = a_2$.

The control algorithm was configured with a reference voltage $u_{\text{ref}} = 230sin(2\pi f_{out}t)$ V, $f_{out} = 50, 150, 500$ Hz; $\Delta U_{tol} = 5$ V.

The system of differential equations was solved using an adaptive-step Runge-Kutta-Fehlberg (RKF45) method [17]. This method automatically adjusts the integration step size to maintain a specified error tolerance, providing both accuracy and computational efficiency. The step size was reduced during the high frequency switching events of the inverter and increased during smoother periods of operation, ensuring a stable solution that accurately

captures all dynamics of the system. The simulations were performed across a range of operating frequencies—50 Hz, 150 Hz, and 500 Hz to assess the technique's robustness under varying conditions.

At 50 Hz, the rectifier stage supplying the DC link operates stably. Rectifier thyristor current pulses (Fig. 2) peak at approximately 0.105 A. These current pulses maintain the rectifier filter capacitor voltage (Fig. 3), which exhibits a characteristic 100 Hz ripple, fluctuating between approximately 275.4 V and 277.9 V. On the inverter side, the load current transient (Fig. 4) exhibits a smooth, damped oscillatory behavior, starting from an initial peak around 6 A and settling toward a steady-state sinusoidal waveform with minimal distortions. Similarly, the voltage transient on the commutating capacitor (Fig. 5) shows a well-controlled decay from approximately 230 V, with oscillations that rapidly attenuate, indicating effective commutation and stable operation. These results demonstrate that the control technique performs excellently at low frequencies, maintaining precise thyristor switching and preventing excessive transients that could lead to component stress or inefficiency.

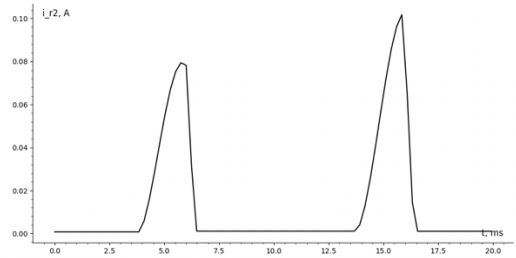

Fig. 2. Rectifier thyristor current pulses at 50 Hz

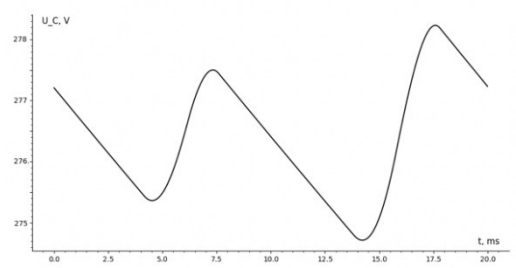

Fig. 3. Voltage transient on the C at 50 Hz

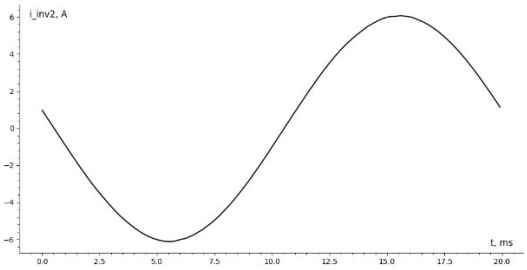

Fig. 4. Load current transient at 50 Hz

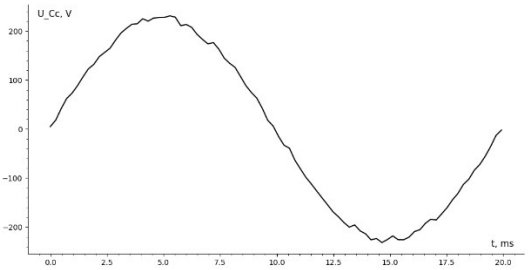

Fig. 5. Voltage transient on the Cc at 50 Hz

Increasing the frequency to 150 Hz, the increased power demand is visible on the rectifier stage. The rectifier current pulses (Fig. 6) are higher, peaking at approximately 0.115 A to supply the required power. This increased load causes the rectifier filter capacitor voltage (Fig. 7) to show a larger ripple and a lower average value, oscillating between approximately 272.7 V and 275.4 V. At this frequency, the load current transient (Fig. 8) displays more pronounced oscillations compared to the 50 Hz case, with peaks reaching about 4.3 A and a slightly extended settling time. However, the waveform remains stable and converges to a clean sinusoidal pattern without significant overshoots or instabilities. The commutating capacitor voltage (Fig. 9) follows a similar trend, starting at around 230 V and showing controlled damping, though with a few additional cycles before stabilization. Overall, the control technique continues to function effectively at this mid-range frequency, highlighting its suitability for applications requiring moderate frequency conversion while preserving system reliability.

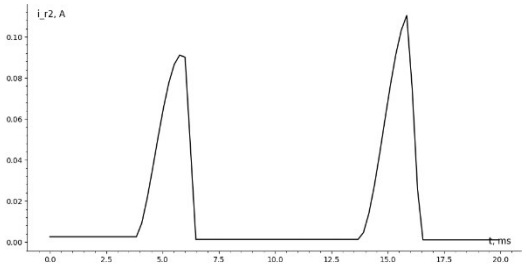

Fig. 6. Rectifier thyristor current pulses at 150 Hz

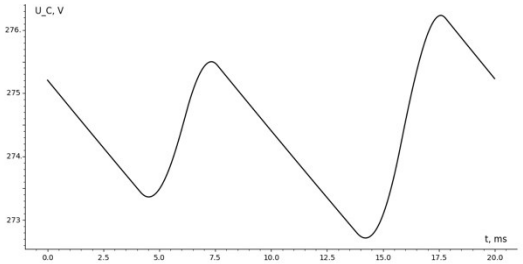

Fig. 7. Voltage transient on the C at 150 Hz

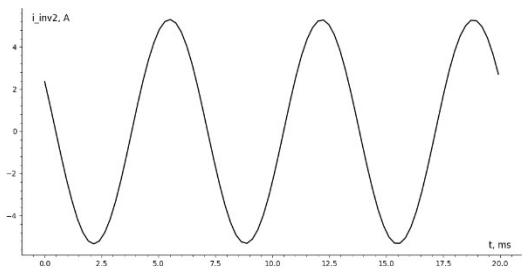

Fig. 8. Load current transient at 150 Hz

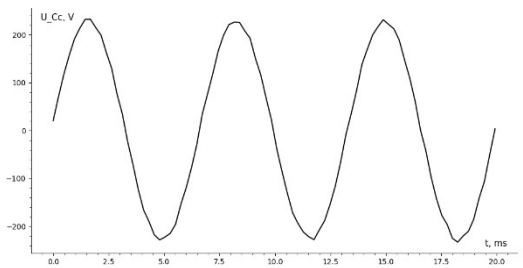

Fig. 9. Voltage transient on the Cc at 150 Hz

When pushed to a high-frequency (500 Hz) output, the significant load on the DC link is evident. To deliver the required power, the rectifier thyristor current (Fig. 10) flows in much stronger pulses, with a peak amplitude reaching approximately 0.18 A. This high power draw causes the rectifier filter voltage (Fig. 11) to see a pronounced drop, with its average value settling lower, around 264 V, and fluctuating between 262.7 V and 265.4 V. The load current (Fig. 12) stabilizes almost instantaneously into a high-quality sinusoidal waveform with an amplitude of approximately 2.3 A and no visible distortion. Concurrently, the commutating capacitor voltage (Fig. 13) clearly illustrates the efficacy of the hysteresis control. The actual voltage is consistently and rapidly switched to remain strictly within the predefined tolerance band around the 500 Hz sinusoidal reference. This result confirms the control strategy's capability to maintain precise waveform synthesis even at significantly higher operating frequencies, validating the model's stability and the control's fast dynamic response.

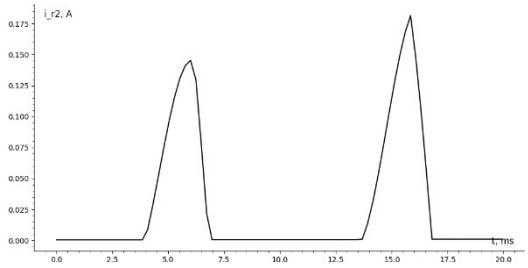

Fig. 10. Rectifier thyristor current pulses at 500 Hz

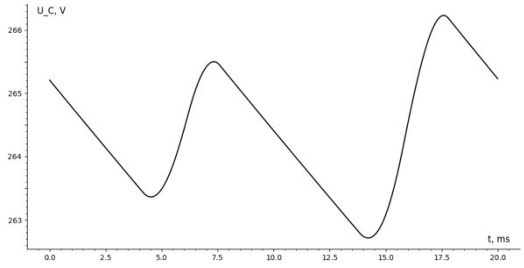

Fig. 11. Voltage transient on the C at 500 Hz

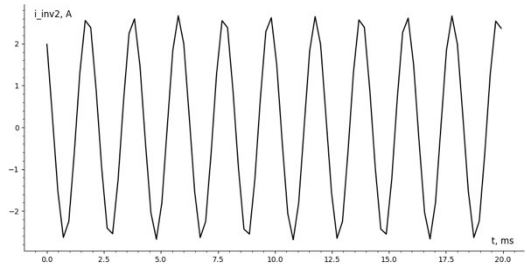

Fig. 12. Load current transient at 500 Hz

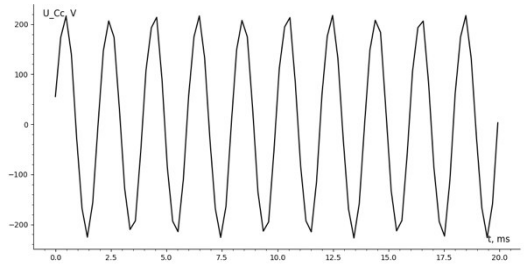

Fig. 13. Voltage transient on the Cc at 500 Hz

Conclusions from this research and prospects for further research in this direction

This study successfully developed a comprehensive mathematical model and an effective hysteresis control technique for a single-phase thyristor frequency converter, enabling the accurate synthesis of arbitrary output voltage waveforms. The state-space model, which utilizes nonlinear equations and logical variables, proved highly effective in capturing the converter's complex, variable-topology dynamics. The control strategy, combining phase-angle control for the rectifier and hysteresis control for the inverter, was validated through numerical simulation.

The simulation results demonstrated high waveform fidelity and fast, stable transient responses across a wide operational range. At lower frequencies (50 Hz and 150 Hz), the system exhibited smooth, well-damped oscillations that settled rapidly, confirming the control's stability. Critically, the system also demonstrated exceptional robustness and high-fidelity tracking at a high output frequency of 500 Hz. At this frequency, the hysteresis control consistently and rapidly forced the output voltage to track the reference signal, producing a high-quality sinusoidal load current without the resonance issues that can affect such topologies.

This work fills a notable research gap by successfully applying non-linear hysteresis control to a thyristor-based topology for precise waveform generation. The results confirm that this approach can achieve a dynamic response superior to traditional linear PWM methods, enhancing power quality for grid-connected renewable systems and industrial applications.

Future research directions include the experimental validation of these simulation results on a hardware prototype to confirm the model's real-world accuracy and control performance. Further work could also focus on extending this model and control strategy to multi-phase systems and investigating adaptive or hybrid control schemes to optimize the variable switching frequency, with a goal of minimizing switching losses and electromagnetic interference. Finally, the integration of intelligent algorithms for automated parameter tuning could further enhance system performance and component selection for specific high-frequency applications.

References

1. Rojas, D., Muñoz, J., Rivera, M., & Rohten, J. (2021). Review of Control Techniques in Microinverters. *Sensors, 21*(19), 6486. https://doi.org/10.3390/s21196486

2. Chatterjee, A., & Mohanty, K. (2018). Current control strategies for single phase grid integrated inverters for photovoltaic applications: A review. *Renewable and Sustainable Energy Reviews, 92*, 551–567. https://doi.org/10.1016/j.rser.2018.04.115

3. Mao, P., Zhang, M., Cui, S., Zhang, W., & Kwon, B.-H. (2014). A review of current control strategy for

single-phase grid-connected inverters. *TELKOMNIKA (Telecommunication Computing Electronics and Control), 12*(3), 563–580. https://doi.org/10.12928/TELKOMNIKA.v12i3.94

4. Jin, J., Chen, T., Luo, L., & Su, S. (2014). A control strategy for single-phase grid-connected inverter with power quality regulatory function. *TELKOMNIKA Indonesian Journal of Electrical Engineering, 12*(1), 33–40. https://doi.org/10.11591/telkomnika.v12i1.3911

5. Rai, S. S., & Pandey, A. K. (2015). A comparative study of various PWM techniques. *International Journal of Engineering Research & Technology, 4*(11), 323–327. https://doi.org/10.17577/IJERTV4IS110125

6. İşen, E. (2021). Comparative study of single-phase PWM rectifier control techniques. *Mugla Journal of Science and Technology, 7*(1), 44–51. https://doi.org/10.22531/muglajsci.870989

7. Chaves, E. N., Coelho, E. A. A., Viajante, G. P., Freitas, L. C. G., Wezs, L. G., Freitas, L. C., Queiroz, C. A., & Bernadeli, V. R. (2016). A control strategy design applied to single-phase grid-connected inverters. *Renewable Energy and Power Quality Journal, 1*(14), Article 441. https://doi.org/10.24084/repqj14.441

8. Jamwal, P., & Singh, S. (2015). Comparative analysis of hysteresis and PWM current controllers for PMSM drive. *International Journal of Modern Engineering Research, 7*(5), 24–28.

9. Subramanian, G., Mishra, M. K., Jayaprakash, K., & Sureshbabu, P. J. (2018). Simulation study of hysteresis current controlled single phase inverters for photovoltaic systems with reduced harmonics level. *International Journal of Applied Engineering Research, 13*(6), 4409–4414.

10. Dwivedi, A., & Tiwari, A. N. (2017). Analysis of three-phase PWM rectifiers using hysteresis current control techniques: A survey. *International Journal of Power Electronics, 8*(4), 349–367. https://doi.org/10.1504/IJPELEC.2017.085201

11. Rodriguez, J., Pontt, J., Silva, C., Correa, P., Lezana, P., Cortes, P., & Ammann, U. (2007). Predictive current control of a voltage source inverter. *IEEE Transactions on Industrial Electronics, 54*(1), 495–503. https://doi.org/10.1109/TIE.2006.888802

12. IndMALL. (2023, December 3). *What is a GTO and IGBT? Explained*. Retrieved September 24, 2025, from https://www.indmall.in/faq/what-is-a-gto-and-igbt/

13. Bernet, S., Teichmann, R., Zuckerberger, A., & Steimer, P. K. (1999). Comparison of high-power IGBTs and hard-driven GTOs for high-power inverters. *IEEE Transactions on Industry Applications, 35*(2), 487–495. https://doi.org/10.1109/28.753645

14. Visicomm Industries. (2024, May 13). *IGBT vs. thyristors: What are the key differences?*. Retrieved September 24, 2025, from https://50hz.com/igbt-vs-thyristors-what-are-the-key-differences/

15. Nevsemi Electronics. (2023, September 26). *IGBT vs GTO: Difference between IGBT and GTO*. Retrieved September 24, 2025, from https://www.nevsemi.com/blog/igbt-vs-gto

16. Steimer, P. K., Grüning, H. E., Werninger, J., Carroll, E., Klaka, S., & Linder, S. (1999). IGCT—a new emerging technology for high power, low cost inverters. *IEEE Industry Applications Magazine, 5*(4), 12–18. https://doi.org/10.1109/2943.771362

17. Fehlberg, E. (1968). Classical fifth-, sixth-, seventh-, and eighth-order Runge-Kutta formulas with stepsize control (NASA TR R-287). National Aeronautics and Space Administration.